Mathematics and Mechanics of Solids
http://mms.sagepub.com/

A direct particle-based computational framework for electrically enhanced thermo-mechanical sintering of powdered materials

TI Zohdi

Mathematics and Mechanics of Solids published online 21 October 2013
DOI: 10.1177/1081286513505472

The online version of this article can be found at:
http://mms.sagepub.com/content/early/2013/10/20/1081286513505472

Published by:
SAGE
http://www.sagepublications.com

Additional services and information for *Mathematics and Mechanics of Solids* can be found at:

Email Alerts: http://mms.sagepub.com/cgi/alerts

Subscriptions: http://mms.sagepub.com/subscriptions

Reprints: http://www.sagepub.com/journalsReprints.nav

Permissions: http://www.sagepub.com/journalsPermissions.nav

>> OnlineFirst Version of Record - Oct 21, 2013

What is This?

Downloaded from mms.sagepub.com at UNIV CALIFORNIA BERKELEY LIB on November 7, 2013

Article

MMS

Mathematics and Mechanics of Solids
1–21
©The Author(s) 2013
Reprints and permissions:
sagepub.co.uk/journalsPermissions.nav
DOI: 10.1177/1081286513505472
mms.sagepub.com
SAGE

A direct particle-based computational framework for electrically enhanced thermo-mechanical sintering of powdered materials

TI Zohdi
Department of Mechanical Engineering, University of California, Berkeley, CA

Received 11 May 2013; accepted 15 June 2013

Abstract
As a method for bonding powdered materials, sintering has distinct advantages, such as the production of a near final-shape of the desired product, without the need for significant post-processing. However, sintering has certain deficiencies, such as incomplete or weak bonding. Research is ongoing to improve the process. One approach to improve sintering processes of powdered materials is via electrically enhanced bonding, whereby electricity is pumped through the material, while it is compressed in a press, in order to induce Joule-heating. This paper develops a computationally based model for the direct simulation of electrically enhanced sintering of powdered materials using particle-based methods. The overall approach is to construct three coupled sub-models which primarily involve: (a) *particle-to-particle mechanical contact*, (b) *particle-to-particle thermal exchange* and (c) *particle-to-particle electrical current flow*. These physical processes are strongly coupled, since the dynamics dictates which particles are in contact and the contacts determine the electrical flow. The flow of electricity controls the Joule-heating and the induced thermal fields, which soften the material, leading to enhanced particle binding. The strong multiphysics-coupled sub-models are solved iteratively within each time-step using a recursive staggering scheme, which employs temporal adaptivity to control the error. If the process does not converge (to within an error tolerance) within a preset number of iterations, the time-step is adapted (reduced) by utilizing an estimate of the spectral radius of the coupled system. The modular approach allows for easy replacement of submodels, if needed. Numerical examples are provided to illustrate the model and numerical solution scheme.

Keywords
Sintering, powders, Joule-heating

1. Introduction

1.1. Basic process

Over 50% of the raw materials handled in industry appear in powdered form during the various stages of processing. One commonly used approach used in processing powdered materials is sintering. Generally, sintering refers to processing a powdered material, comprised of fine-scale particles, by compacting it in a press (Figure 1) and utilizing heat to bind the material. Sintering has distinct advantages over other methods, for example (a) high purity of processed materials, (b) relatively few steps in fabrication (thus retaining the purity)

Corresponding author:
TI Zohdi, Department of Mechanical Engineering, University of California, Berkeley, CA, 94720-1740, USA.
Email: zohdi@me.berkeley.edu

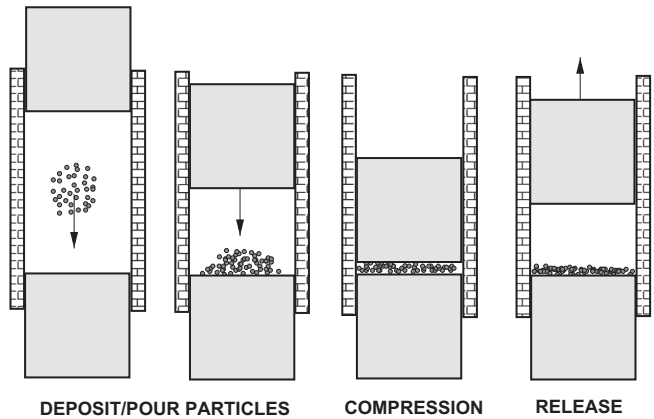

Figure 1. *A model problem:* The sequence of events: (a) particles dropped onto a surface; (b) an electrified head compresses and electrifies the particles; (c) the particles heat up and fuse together; and (d) the electrified head is removed.

and (c) the production of near net-shape of the desired product. Most importantly it is a method that can be utilized to produce products with complex shapes that cannot be easily made with other methods. Innovative methods for processing compacted microscale powders are rapidly being developed in industry in order to meet the specifications demanded by new products.

The delivery of heat can be achieved in a variety of ways, for example, by heating the walls of the press, with the heat transfer taking place primarily by thermal conduction. In an effort to enhance the heat transfer process, in particular within the interior of the material to be processed, electrically aided heat generation, drawing upon the material's inherent resistance, via Joule-heating, is one method, and is considered in this work.[1]

Remark: Consistent, high-quality, particles can be produced in a variety of ways, for example:

- melting and vaporizing of metals and other materials, and harvesting the subsequent particles;
- atomization of liquid streams into droplets by breaking jets of metal;
- reduction of metal oxides; and
- comminution/pulverizing of bulk material.

The particles are usually passed through a series of sieves to separate particles of various sizes.

1.2. Objectives

The objective in this paper is to develop a direct particle-based model which captures three main physical events:

- *particle dynamics*, which primarily entails: (a) the movement of the particles induced by contact with the compressing walls and (b) particle-to-particle contact forces;
- *particle electrical current flow*, which primarily entails: (a) current flow through the particles and (b) current exchange between the particles and walls;
- *particle thermodynamics,* which primarily entails: (a) heat generation via Joule-heating, (b) heat transfer between particles in contact by conduction and (c) thermal softening of the particles.

This is a strongly coupled multiphysical system, since the dynamics controls which particles are in mechanical contact, thus dictating the electrical contacts, which in turn controls the Joule-heating and the induced thermal fields, thus softening and binding the material. The approach taken in the present work is to construct a sub-model for each primary physical process. These submodels are coupled to one another. In order to resolve the coupling, a recursive multiphysical staggering scheme is constructed. The general methodology is as follows (at a given time increment): (1) each field equation is solved individually, "freezing" the other (coupled) fields in the system, allowing only the primary field to be active; and (2) after the solution of each field equation, the primary field variable is updated, and the next field equation is treated in a similar manner. As the physics changes, the field that is most sensitive (exhibiting the largest amount of relative nondimensional change) dictates the time-step size. This approach can be classified as an implicit, staggered, time-stepping scheme, in conjunction with an iterative solution method that automatically adapts the time-step sizes to control the rates of convergence within

a time-step. If the process does not converge (below an error tolerance) within a preset number of iterations, the time-step is adapted (reduced) by utilizing an estimate of the spectral radius of the coupled system. The modular approach allows for easy replacement of submodels, if needed.

Remark 1: The approach outlined here is can be thought of as a *middle ground* between semi-analytical approaches which provide qualitative information [1] and computationally expensive "brute-force" continuum approaches [2, 3] which attempt to resolve the evolution of fine-scale thermal gradients, transient electromagnetic fields, stress fields and chemical/damage fields by solving a coupled system of PDE's associated with (a) Maxwell's equations, (b) the first law of thermodynamics, (c) the balance of linear momentum and (d) reaction-diffusion laws. For the mentioned "brute-force" continuum approach to accurately resolve the coupled time-transient spatial electromagnetic, thermal, mechanical and chemical fields, Zohdi [2] developed a staggered, temporally adaptive, FDTD (Finite Difference Time Domain) method. This is a computationally intensive approach, owing to the fact that one needs literally millions of numerical unknowns, due to the fine mesh sizes needed. We remark that there are other continuum-based methods, such as (a) *the Multi Resolution Time Domain Method*, which is based on wavelet-based discretization, (b) *the Finite Element Method*, which is based on discretization of variational formulations and which are ideal for irregular geometries (see Demkowicz et al. [4, 5] for the state of the art in adaptive Finite Element Methods for Maxwell's equations), (c) *the Pseudo Spectral Time Domain Method*, which is based on Fourier and Chebyshev transforms, followed by a lattice or grid discretization of the transformed domain (d) *the Discrete Dipole Approximation*, which is based on an array of dipoles solved iteratively with the Conjugate Gradient method and a Fast Fourier Transform to multiply matrices, (e) *the Method of Moments*, which is based on integral formulations employing Boundary Element Method discretization, often accompanied by the Fast Multipole Method to accelerate summations needed during the calculations, and (f) *the Partial Element Equivalent Circuit Method*, which is based on integral equations that are interpreted as circuits in discretization cells. However, they are also primarily based on continuum models, and are computationally intensive.

Remark 2: There has been considerable research activity in *non-electrical* compaction of powders, for example, see Akisanya et al. [6], Anand and Gu [7], Brown and Abou-Chedid [8], Domas [9], Fleck [10], Gethin et al., [11], Gu et al. [12], Lewis et al. [13], Ransing et al. [14], Tatzel [15] and Zohdi [16, 17]. The study of "granular" or "particulate" media, in the absence of electrical effects, is wide ranging. Classical examples include the study of natural materials, such as sand and gravel, associated with coastal erosion, landslides and avalanches. For reviews see, for example, Duran [18], Pöschel and Schwager [19], the works of Torquato and collaborators (Torquato [20], Kansaal et al. [21] and Donev et al. [22–26]), the works of Onate and collaborators (Onate et al. [27, 28], Rojek et al. [29], Carbonell et al. [30] and Labra and Onate [31]), Jaeger and Nagel [32, 33], Nagel [34], Liu et al. [35], Liu and Nagel [36], Jaeger and Nagel [37], Jaeger et al. [38–40], Jaeger and Nagel [41], the extensive works of Hutter and collaborators (Tai et al. [42–44], Gray et al. [45], Wieland et al. [46], Berezin et al. [47], Gray and Hutter [48], Gray [49], Hutter [50], Hutter et al. [51], Hutter and Rajagopal [52], Koch et al. [53], Greve and Hutter [54] and Hutter et al. [55]; the works of Behringer and collaborators (Behringer [56], Behringer and Baxter [57], Behringer and Miller [58] and Behringer et al. [59]) and the works of Jenkins and collaborators (Jenkins and Strack [60], Jenkins and La Ragione [61], Jenkins and Koenders [62] and Jenkins et al. [63]).

Remark 3: To predict the resulting effective bulk properties of the final sintered product, there exist several methods dating back well over 150 years, for example to Maxwell [64, 65] and Lord Rayleigh [66]. For a thorough analysis of many of such methods, see Torquato [20], Jikov et al. [67], Hashin [68] and Nemat-Nasser and Hori [69] for solid-mechanics oriented treatments, and Ghosh [70], Ghosh and Dimiduk [71] and Zohdi and Wriggers [72] for computational aspects.

2. Direct particle representation

The objects in the powder-system are assumed to be small enough to be considered (idealized) as particles, spherical in shape, and that the effects of their rotation with respect to their mass center is unimportant to their overall motion. We consider a group of non-intersecting particles ($i = 1, 2, \ldots, N_p$). The equation of motion for the ith particle in system is

$$m_i \ddot{\boldsymbol{r}}_i = \boldsymbol{\Psi}_i^{tot}(\boldsymbol{r}_1, \boldsymbol{r}_2, \ldots, \boldsymbol{r}_{N_p}) = \boldsymbol{\Psi}_i^{con} + \boldsymbol{\Psi}_i^{fric} + \boldsymbol{\Psi}_i^{wall} + \boldsymbol{\Psi}_i^{bond} + \boldsymbol{\Psi}_i^{env}, \tag{1}$$

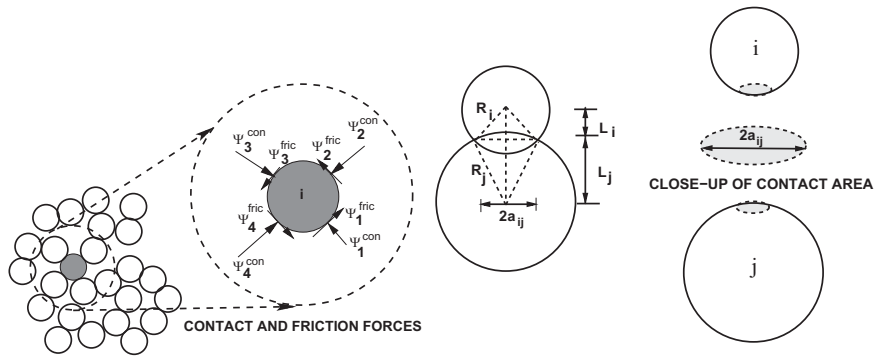

Figure 2. *Left*: Normal contact and friction forces. *Right*: An approximation of the contact area parameter for two particles in contact.

where $\boldsymbol{r}_i$ is the position vector of the ith particle and where $\boldsymbol{\Psi}_i^{tot}$ represents all forces acting on particle i, which is decomposed into the sum of forces due to normal contact forces ($\boldsymbol{\Psi}_i^{con}$), sliding frictional forces ($\boldsymbol{\Psi}_i^{fric}$), wall forces ($\boldsymbol{\Psi}_i^{wall}$, having both contact and friction), adhesive bonding forces ($\boldsymbol{\Psi}_i^{bond}$) with other particles and forces arising from the surrounding interstitial environment ($\boldsymbol{\Psi}_i^{env}$).[2] In the next sections, we elaborate each of the types of forces in the system in detail.

2.1. Particle-to-particle contact forces

We employ a simple particle overlap model to determine the force contributions from the surrounding particles (N_{ci}) in contact, $\boldsymbol{\Psi}_i^{con} = \sum_{j=1}^{N_{ci}} \boldsymbol{\Psi}_{ij}^{con}$, based on a normalized separation distance between particles in contact (Figure 2). We assume that the contact force is proportional to the relative *normalized* proximity of the particles. For example, a simple relation for particles in contact ($||\boldsymbol{r}_i - \boldsymbol{r}_j|| \leq R_i + R_j$) is

$$\boldsymbol{\Psi}_{ij}^{con} \propto -K_p |\mathcal{E}_{ij}|^{p_p} \boldsymbol{n}_{ij} A_{ij}^c, \tag{2}$$

where $0 < K_p < \infty$ is a particle-to-particle contact compliance constant, p_p is a material parameter, $\mathcal{E}_{ij}$ is normalized/nondimensional (strain-like) deformation metric

$$\mathcal{E}_{ij} = \frac{||\boldsymbol{r}_i - \boldsymbol{r}_j|| - (R_i + R_j)}{(R_i + R_j)} \tag{3}$$

and

$$\boldsymbol{n}_{ij} = -\frac{\boldsymbol{r}_i - \boldsymbol{r}_j}{||\boldsymbol{r}_i - \boldsymbol{r}_j||} = \frac{\boldsymbol{r}_j - \boldsymbol{r}_i}{||\boldsymbol{r}_i - \boldsymbol{r}_j||}, \tag{4}$$

where the R_i and R_j are the radii of particles i and j respectively. For the generated friction, we assume a simple contact-induced sliding friction relation:

$$\boldsymbol{\Psi}_{ij}^{fric} = \mu_d ||\boldsymbol{\Psi}_{ij}^{con}|| \boldsymbol{t}_{ij}, \tag{5}$$

where

$$\boldsymbol{t}_{ij} = -\frac{\boldsymbol{v}_i - \boldsymbol{v}_j}{||\boldsymbol{v}_j - \boldsymbol{v}_i||} = \frac{\boldsymbol{v}_j - \boldsymbol{v}_i}{||\boldsymbol{v}_j - \boldsymbol{v}_i||}, \tag{6}$$

and where A_{ij}^c is the contact area parameter, which is derived next.

Remark: One could can easily construct more elaborate relations connecting the relative proximity of the particles and other metrics to the contact force, $\boldsymbol{\Psi}_{ij}^{con} \propto \mathcal{F}(\boldsymbol{r}_i, \boldsymbol{r}_j, \boldsymbol{n}_{ij}, R_i, R_j, \ldots)$, building on Hertzian contact models. This poses no difficulty in the direct numerical method developed. For much more detailed constitutive relations between particles, see Zohdi [73]. For the remainder of the analysis, we shall use the deformation metric in equation (3).

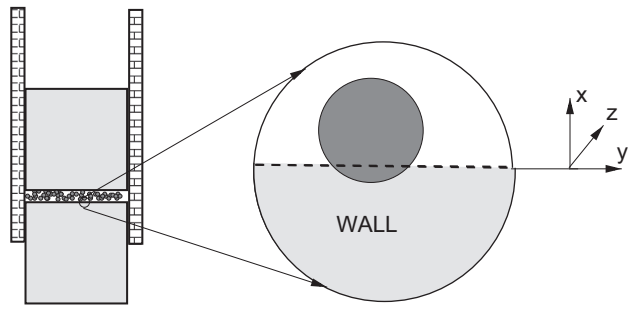

Figure 3. An example of overlap contact between the wall and a particle. The amount of overlap of the particle with the wall position dictating the force.

2.1.1. Contact area parameter. Referring to Figure 2, one can solve for an approximation of the common contact radius a_{ij} (and the contact area, $A^c_{ij} = \pi a^2_{ij}$) by solving the following three equations:

$$a^2_{ij} + L^2_i = R^2_i, \tag{7}$$

and

$$a^2_{ij} + L^2_j = R^2_j, \tag{8}$$

and

$$L_i + L_j = ||\boldsymbol{r}_i - \boldsymbol{r}_j||, \tag{9}$$

where R_i is the radius of particle i, R_j is the radius of particle j, L_i is the distance from the center of particle i and the common contact interpenetration line and L_j is the distance from the center of particle j and the common contact interpenetration line, where the extent of interpenetration is

$$\delta_{ij} = R_i + R_j - ||\boldsymbol{r}_i - \boldsymbol{r}_j||. \tag{10}$$

Solving these equations leads to

$$A^c_{ij} = \pi a^2_{ij} = \pi(R^2_i - L^2_i), \tag{11}$$

where

$$L_i = \frac{1}{2}\left(||\boldsymbol{r}_i - \boldsymbol{r}_j|| - \frac{R^2_j - R^2_i}{||\boldsymbol{r}_i - \boldsymbol{r}_j||}\right). \tag{12}$$

Remark: It is obvious that for a deeper understanding of the deformation within a particle, it must be treated as a deformable continuum, which would require a highly resolved spatial discretization, for example using the Finite Element Method for the contacting bodies. This requires a large computational effort. For the state of the art in Finite Element Methods, see the recent book of Wriggers [74]. For work specifically focusing on the continuum mechanics of particles, see Zohdi and Wriggers [72]. For a detailed numerical analysis of multifield contact between bodies, see Wriggers [75].

2.2. Particle-to-wall contact

The contact between the wall and the particles is handled exactly in the same manner as the particle to particle contact, with the amount of overlap of the particle with the wall position dictating the force. For example (see Figure 3), if $||r_{xi}|| \geq W_x$, then

$$\boldsymbol{\Psi}^{wall,con}_i \propto -K_w|\mathcal{E}_{iw}|^{p_w}\boldsymbol{n}_{iwx}A^c_i, \tag{13}$$

where $0 < K_w < \infty$ is a wall-to-particle compliance constant, p_w is a material constant and

$$\mathcal{E}_{iw} = \frac{W_x - r_{xi}}{R_i} \tag{14}$$

and

$$\boldsymbol{n}_{iwx} = \frac{W_x - r_{xi}}{|W_x - r_{xi}|}\boldsymbol{e}_x, \tag{15}$$

where $\boldsymbol{e}_x$ is the unit normal in the x-direction. The same holds for other components and walls. For the generated friction, we assume, continuous sliding:

$$\boldsymbol{\Psi}_{ij}^{fric} = \mu_d ||\boldsymbol{\Psi}^{wall,con}||\boldsymbol{t}_{iw}, \tag{16}$$

where

$$\boldsymbol{t}_{iw} = \frac{\boldsymbol{v}_{w,t} - \boldsymbol{v}_{i,t}}{||\boldsymbol{v}_{w,t} - \boldsymbol{v}_{i,t}||}, \tag{17}$$

where the subscript t denotes the tangential component.

Remark: The parameters K_p and K_w can thermally soften, and this is discussed later in the numerical examples.

2.3. Particle-to-particle bonding relation

For the particles to bond, we adopt a criteria based on exceeding a critical interpenetration distance. Explicitly:

- If $||\boldsymbol{r}_i - \boldsymbol{r}_j|| \leq (R_i + R_j)$, then the particles are in contact and we have

$$\mathcal{E}_{ij} = \frac{||\boldsymbol{r}_i - \boldsymbol{r}_j|| - (R_i + R_j)}{(R_i + R_j)}. \tag{18}$$

- If $\mathcal{E}_{ij} \leq 0$, and $|\mathcal{E}_{ij}| \geq \mathcal{E}^*$, then an (adhesive) bond is activated between the particles of the form

$$\boldsymbol{\Psi}_{ij}^{bond} = K_b|\mathcal{E}_{ij}|^{p_b}\boldsymbol{n}_{ij}A_{ij}^c, \tag{19}$$

  where $0 \leq K_b$ is a bonding constant, and p_b is a material parameter.
- If $||\boldsymbol{r}_i - \boldsymbol{r}_j|| \geq (R_i + R_j)$, then $\mathcal{E}_{ij} > 0$, since there is no contact.

2.4. Interstitially induced particle drag

A possible source of environmental forces is due to damping from interstitial fluid between particles, such as binding enhancers, surfactants and lubricants. A simple model to account for this is

$$\boldsymbol{\Psi}_i^{env} = -c^{env}(\boldsymbol{v}_i - \boldsymbol{v}^{env}) \tag{20}$$

where $\boldsymbol{v}_i$ is the velocity of the ith particle and $\boldsymbol{v}^{env}$ is the local velocity of the interstitial medium, which one may assume to be $\boldsymbol{v}^{env} \approx \boldsymbol{0}$. The mechanics of the interstitial fluid are unimportant in these problems. However, for other applications, such as high-speed flow, the motion of the fluid can be important, necessitating fully coupled (two-way) particle-fluid interaction models. This is outside the scope of the present work. Generally, this requires the use of solid-fluid staggering-type schemes (for example, see Zohdi [76]).

2.5. Total forces acting on particles

In summary, we have the following forces acting on each particle ($i = 1, 2, \ldots, N_p$)

$$\boldsymbol{\Psi}_i^{tot} \stackrel{\text{def}}{=} \boldsymbol{\Psi}_i^{con} + \boldsymbol{\Psi}_i^{fric} + \boldsymbol{\Psi}_i^{wall} + \boldsymbol{\Psi}_i^{bond} + \boldsymbol{\Psi}_i^{env}. \tag{21}$$

The three material contact compliance constants are functions of temperature, $K_p = K_p(\theta)$, $K_w = K_w(\theta)$ and $K_b = K_b(\theta)$, and the temperature is, in turn, a function of the Joule-heating, $\theta(\boldsymbol{J})$, where $\boldsymbol{J}$ is the current. We will discuss the thermo-electric effects shortly, but first indicate how the preceding dynamical particle system can solved.

3. Time-stepping

Integrating equation (1) leads to (using a trapezoidal rule with variable integration metric, $0 \leq \phi \leq 1$)

$$\begin{aligned} \boldsymbol{v}_i(t+\Delta t) &= \boldsymbol{v}_i(t) + \frac{1}{m_i}\int_t^{t+\Delta t} \boldsymbol{\Psi}_i^{tot}\, dt \\ &\approx \boldsymbol{v}_i(t) + \frac{\Delta t}{m_i}\left(\phi \boldsymbol{\Psi}_i^{tot}(t+\Delta t) + (1-\phi)\boldsymbol{\Psi}_i^{tot}(t)\right). \end{aligned} \tag{22}$$

The position can be computed via application of the trapezoidal rule again:

$$\boldsymbol{r}_i(t+\Delta t) \approx \boldsymbol{r}_i(t) + \Delta t(\phi \boldsymbol{v}_i(t+\Delta t) + (1-\phi)\boldsymbol{v}_i(t)), \tag{23}$$

which can be consolidated into

$$\boldsymbol{r}_i(t+\Delta t) = \boldsymbol{r}_i(t) + \boldsymbol{v}_i(t)\Delta t + \frac{\phi(\Delta t)^2}{m_i}\left(\phi \boldsymbol{\Psi}_i^{tot}(t+\Delta t) + (1-\phi)\boldsymbol{\Psi}_i^{tot}(t)\right). \tag{24}$$

This leads to a coupled system of equations, which are solved using an adaptive iterative scheme, building on approaches found in various forms in Zohdi [77, 78].

3.1. Iterative (implicit) solution method

Following the basic framework in Zohdi [77], [78], we write equation (24) in a slightly more streamlined form for particle i

$$\boldsymbol{r}_i^{L+1} = \boldsymbol{r}_i^{L} + \boldsymbol{v}_i^{L}\Delta t + \frac{\phi(\Delta t)^2}{m_i}\left(\phi(\boldsymbol{\Psi}_i^{tot,L+1}) + (1-\phi)(\boldsymbol{\Psi}^{tot,L})\right), \tag{25}$$

which leads to a coupled set equations for $i = 1, 2, \ldots, N_p$ particles.[3] The set of equations represented by equation (25) can be solved recursively. equation (25) can be solved recursively by recasting the relation as

$$\boldsymbol{r}_i^{L+1,K} = \boldsymbol{r}_i^{L} + \boldsymbol{v}_i^{L}\Delta t + \frac{(\phi\Delta t)^2}{m_i}\boldsymbol{\Psi}_i^{tot,L+1,K-1} + \frac{\phi(\Delta t)^2}{m_i}(1-\phi)\boldsymbol{\Psi}_i^{tot,L}, \tag{26}$$

which is of the form

$$\boldsymbol{r}_i^{L+1,K} = \mathcal{G}(\boldsymbol{r}_i^{L+1,K-1}) + \mathcal{R}_i, \tag{27}$$

where $K = 1, 2, 3, \ldots$ is the index of iteration within time-step $L+1$ and

- $\boldsymbol{\Psi}_i^{tot,L+1,K-1} \stackrel{\text{def}}{=} \boldsymbol{\Psi}_i^{tot,L+1,K-1}(\boldsymbol{r}_1^{L+1,K-1}, \boldsymbol{r}_2^{L+1,K-1}, \ldots, \boldsymbol{r}_N^{L+1,K-1})$,
- $\boldsymbol{\Psi}_i^{tot,L} \stackrel{\text{def}}{=} \boldsymbol{\Psi}_i^{tot,L}(\boldsymbol{r}_1^{L}, \boldsymbol{r}_2^{L}, \ldots, \boldsymbol{r}_N^{L})$,
- $\mathcal{G}(\boldsymbol{r}_i^{L+1,K-1}) = \frac{(\phi\Delta t)^2}{m_i}\boldsymbol{\Psi}_i^{tot,L+1,K-1}$ and
- $\mathcal{R}_i = \boldsymbol{r}_i^{L} + \boldsymbol{v}_i^{L}\Delta t + \frac{\phi(\Delta t)^2}{m_i}(1-\phi)\boldsymbol{\Psi}_i^{tot,L}$.

The term $\mathcal{R}_i$ is a remainder term that does not depend on the solution. The convergence of such a scheme is dependent on the behavior of $\mathcal{G}$. Namely, a sufficient condition for convergence is that $\mathcal{G}$ is a contraction mapping for all $\boldsymbol{r}_i^{L+1,K}$, $K = 1, 2, 3 \ldots$ In order to investigate this further, we define the iteration error as

$$\varpi_i^{L+1,K} \stackrel{\text{def}}{=} \boldsymbol{r}_i^{L+1,K} - \boldsymbol{r}_i^{L+1}. \tag{28}$$

A necessary restriction for convergence is iterative self consistency, i.e. the "exact" (discretized) solution must be represented by the scheme, $\boldsymbol{r}_i^{L+1} = \mathcal{G}(\boldsymbol{r}_i^{L+1}) + \mathcal{R}_i$. Enforcing this restriction, a sufficient condition for convergence is the existence of a contraction mapping

$$||\underbrace{\boldsymbol{r}_i^{L+1,K} - \boldsymbol{r}_i^{L+1}}_{\varpi_i^{L+1,K}}|| = ||\mathcal{G}(\boldsymbol{r}_i^{L+1,K-1}) - \mathcal{G}(\boldsymbol{r}_i^{L+1})|| \leq \eta^{L+1,K}||\boldsymbol{r}_i^{L+1,K-1} - \boldsymbol{r}_i^{L+1}||, \tag{29}$$

where, if $0 \leq \eta^{L+1,K} < 1$ for each iteration K, then $\varpi_i^{L+1,K} \to \mathbf{0}$ for any arbitrary starting value $\boldsymbol{r}_i^{L+1,K=0}$, as $K \to \infty$, which is a contraction condition that is sufficient, but not necessary, for convergence. The convergence of equation (26) is scaled by $\eta \propto \dfrac{(\phi \Delta t)^2}{m_i}$. Therefore, we see that the contraction constant of $\mathcal{G}$ is:

- directly dependent on the magnitude of the interaction forces ($||\boldsymbol{\Psi}||$),
- inversely proportional to the masses m_i and
- directly proportional to $(\Delta t)^2$.

Thus, decreasing the time-step size improves the convergence. *In order to maximize the time-step sizes (to decrease overall computing time) and still meet an error tolerance on the numerical solution's accuracy*, we build on an approach originally developed for continuum thermo-chemical multifield problems (Zohdi [77]), where one assumes: (1) $\eta^{L+1,K} \approx S(\Delta t)^p$, ($S$ is a constant) and (2) the error within an iteration behaves according to $(S(\Delta t)^p)^K \varpi^{L+1,0} = \varpi^{L+1,K}$, $K = 1, 2, \ldots$, where $\varpi^{L+1,0} = \boldsymbol{r}^{L+1,K=1} - \boldsymbol{r}^L$ is the initial norm of the iterative (relative) error and S is intrinsic to the system. For example, for second-order problems, due to the quadratic dependency on Δt, $p \approx 2$. The objective is to meet an error tolerance in exactly a preset (the analyst sets this) number of iterations. To this end, one writes $(S(\Delta t_{\text{tol}})^p)^{K_d} \varpi^{L+1,0} = TOL$, where TOL is a tolerance and where K_d is the number of desired iterations. If the error tolerance is not met in the desired number of iterations, the contraction constant $\eta^{L+1,K}$ is too large. Accordingly, one can solve for a new smaller step size, under the assumption that S is constant,

$$\Delta t_{\text{tol}} = \Delta t \underbrace{\left(\frac{(\frac{TOL}{\varpi^{L+1,0}})^{\frac{1}{pK_d}}}{(\frac{\varpi^{L+1,K}}{\varpi^{L+1,0}})^{\frac{1}{pK}}} \right)}_{\stackrel{\text{def}}{=} \Lambda_K}. \tag{30}$$

The assumption that S is constant is not critical, since the time-steps are to be recursively refined and unrefined throughout the simulation. Clearly, the expression in Equation 30 can also be used for time-step enlargement, if convergence is met in less than K_d iterations (typically chosen to be between 5 to 10 iterations). Specifically, the solution steps are, within a time-step:

1. Start a global fixed iteration (set $i = 1$ (particle counter) and $K = 0$ (iteration counter)).
2. If $i > N_p$ then go to (4).
3. If $i \leq N_p$ then:
   (a) compute the position $\boldsymbol{r}_i^{L+1,K}$;
   (a) go to (2) for the next particle ($i = i + 1$).
4. Measure error (normalized) quantities
   (a) $\varpi_K \stackrel{\text{def}}{=} \dfrac{\sum_{i=1}^{N_p} ||\boldsymbol{r}_i^{L+1,K} - \boldsymbol{r}_i^{L+1,K-1}||}{\sum_{i=1}^{N_p} ||\boldsymbol{r}_i^{L+1,K} - \boldsymbol{r}_i^{L}||}$,
   (b) $Z_K \stackrel{\text{def}}{=} \dfrac{\varpi_K}{TOL_r}$,
   (c) $\Lambda_K \stackrel{\text{def}}{=} \left(\dfrac{(\frac{TOL}{\varpi_0})^{\frac{1}{pK_d}}}{(\frac{\varpi_K}{\varpi_0})^{\frac{1}{pK}}} \right)$.
5. If the tolerance is met: $Z_K \leq 1$ and $K < K_d$, then:
   (a) increment time: $t = t + \Delta t$;
   (b) construct the next time-step: $(\Delta t)^{new} = \Lambda_K (\Delta t)^{old}$;
   (c) select the minimum size: $\Delta t = MIN((\Delta t)^{lim}, (\Delta t)^{new})$ and go to (1).
6. If the tolerance is not met: $Z_K > 1$ and $K < K_d$, then:
   (a) update the iteration counter: $K = K + 1$;
   (b) reset the particle counter: $i = 1$;
   (c) go to (2).

7. If the tolerance is not met ($Z_K > 1$) and $K = K_d$, then:
   (a) construct a new time-step: $(\Delta t)^{new} = \Lambda_K (\Delta t)^{old}$;
   (b) restart at time t and go to (1).

Time-step size adaptivity is critical, since the system's dynamics and configuration can dramatically change over the course of time, possibly requiring quite different time-step sizes to control the iterative error. However, to maintain the accuracy of the time-stepping scheme, one must respect an upper bound dictated by the discretization error, i.e., $\Delta t \leq \Delta t^{lim}$. Note that in step (5), Λ_K may enlarge the time-step if the error is lower than the preset tolerance. The algorithm will be modified shortly to account for coupled thermal and electrical effects.

4. Thermal fields

4.1. Governing equations

We assume that radiative, convective and strain-rate effects are negligible for the particle's thermodynamics. Only Joule-heating and conduction are considered important. Thus, for each particle $i = 1, 2, \ldots, N_p$,

$$m_i C_i \dot{\theta}_i = \mathcal{Q}_i + \mathcal{H}_i, \tag{31}$$

where $\mathcal{Q}_i$ represents the conductive contribution from surrounding particles in contact (including walls), and $\mathcal{H}_i$ represents the Joule-heating term. It is assumed that the temperature fields are uniform within the (small) particles. This assumption is justified, i.e. a lumped thermal model, ignoring temperature gradients and assuming a uniform temperature within a particle, when the Biot number is small. The Biot number for spheres scales with the ratio of the particle volume (V) to the particle surface area (A_s) in the following manner (R being the particle radius)

$$\frac{V}{A_s} = \frac{\frac{4}{3}\pi R^3}{4\pi R^2} = \frac{R}{3}, \tag{32}$$

which indicates that a uniform temperature distribution is appropriate, since the particles, by definition, are small. Assuming that the fields are uniform in each particle allows for the following (for particle i)

$$\mathcal{Q} = -\int_{\partial\omega} \boldsymbol{Q} \cdot \boldsymbol{n}\, dA \approx \sum_{j=1}^{N_{pc}} \mathbb{K}_{ij} \frac{\theta_j - \theta_i}{||\boldsymbol{r}_i - \boldsymbol{r}_j||} A_{ij}^c, \tag{33}$$

where the summation extends over all particles $j = 1, 2, 3, \ldots, N_{pc}$ that are in contact with particle i (Figure 4).[4] This yields

$$m_i C_i \frac{d\theta_i}{dt} = \underbrace{\sum_{j=1}^{N_{pc}} \mathbb{K}_{ij} \frac{\theta_j - \theta_i}{||\boldsymbol{r}_i - \boldsymbol{r}_j||} A_{ij}^c}_{\mathcal{Q}_i} + \mathcal{H}_i, \tag{34}$$

where the specific form of Joule-heating is

$$\mathcal{H}_i \approx a_i \frac{J_i^2}{\sigma_i} V_i, \tag{35}$$

where J_i is the current magnitude in particle i, σ_i is the conductivity and $0 \leq a_i \leq 1$ is an absorption constant. More remarks on Joule-heating will be given shortly.

4.2. Numerical integration

Integrating leads the energy equation yields for each particle ($i = 1, 2, \ldots, N_p$)

$$\begin{aligned} \theta_i(t + \Delta t) &= \theta_i(t) + \frac{1}{m_i C_i} \left(\int_t^{t+\Delta t} \mathcal{Q}_i\, dt + \int_t^{t+\Delta t} \mathcal{H}_i\, dt \right) \\ &\approx \theta_i(t) + \frac{\Delta t}{m_i C_i} \left(\phi(\mathcal{Q}_i(t + \Delta t) + \mathcal{H}_i(t + \Delta t)) + (1 - \phi)(\mathcal{Q}_i(t) + \mathcal{H}_i(t)) \right). \end{aligned} \tag{36}$$

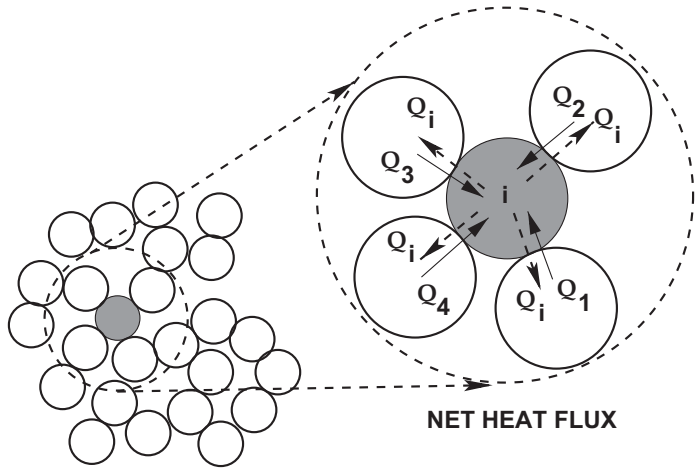

Figure 4. Heat flux exchange between particles.

We note that equation (36) represents a coupled system of the general form (similar to the equation that arises for the particle dynamics)

$$\theta_i(t+\Delta t) = \mathcal{G}_i(\theta_i(t+\Delta t)) + \mathcal{R}_i, \tag{37}$$

where for the "remainder" term, $\mathcal{R}_i \neq \mathcal{R}_i(\theta_i(t+\Delta t))$, and where $\mathcal{G}_i$'s behavior is controlled by the magnitude of Δt. Clearly, the temperature is coupled to the mechanical behavior of the system. Shortly, we develop a multiphysical staggering scheme to solve the overall system.

5. Modeling of current flow

5.1. Particle model simplification

In order to describe the electrical flow in the system, we consider a conservation of charge in integral form (posed over an arbitrary, general, domain ω)

$$\int_{\partial\omega} \boldsymbol{J}\cdot\boldsymbol{n}\,dA + \int_{\omega} \frac{\partial \mathcal{P}}{\partial t}\,dV = 0, \tag{38}$$

where $\boldsymbol{J}$ is the current field and $\mathcal{P}$ is the charge. We assume that the electrical current has evolved to steady state on time-scales that are much shorter than the dynamics of the particles (see Appendix B for justification). Therefore, $\frac{\partial \mathcal{P}}{\partial t} = 0$ is assumed throughout the remainder of this work; thus,

$$\int_{\partial\omega} \boldsymbol{J}\cdot\boldsymbol{n}\,dA = 0. \tag{39}$$

For the particle model, we re-express equation (39) in terms of electrical contact and current flow (through the particle interfaces), characterized by fluxes in and out of particles, as

$$\sum_{j=1}^{N_{pc}} (\boldsymbol{J}_i + \boldsymbol{J}_j)\cdot\boldsymbol{n}_{ij}A^c_{ij} = 0, \tag{40}$$

where A^c_{ij} is the contact area associated with the particle pair (ij), $\boldsymbol{n}_{ij} = \frac{\boldsymbol{r}_j-\boldsymbol{r}_i}{||\boldsymbol{r}_i-\boldsymbol{r}_j||}$ and N_{pc} is the number of particles in contact with particle i. Assuming that the current flows in and out in a radial manner,

$$(\boldsymbol{J}_i + \boldsymbol{J}_j) = (J_i - J_j)\boldsymbol{n}_{ij}. \tag{41}$$

Thus,

$$\sum_{j=1}^{N_{pc}} (J_i - J_j)A^c_{ij} = 0 \Rightarrow J_i = \frac{\sum_{j=1}^{N_{pc}} J_j A^c_{ij}}{\sum_{j=1}^{N_{pc}} A^c_{ij}}. \tag{42}$$

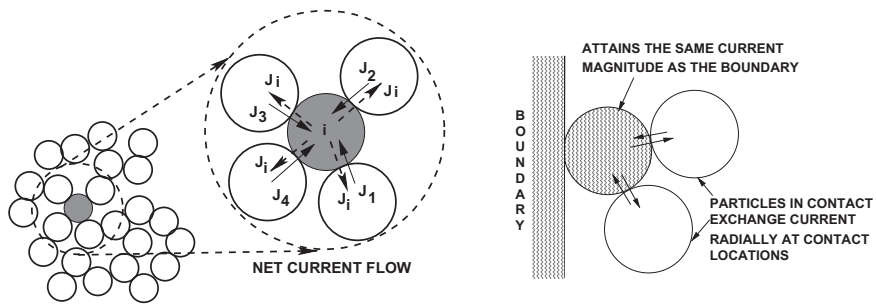

Figure 5. *Left*: Current exchange between particles. *Right*: The particles in contact with the walls are assumed to become fully electrified and to attain the magnitude of current in the wall as well as the temperature of the wall. From particles that contact the walls, the current flows radially to contact pairs.

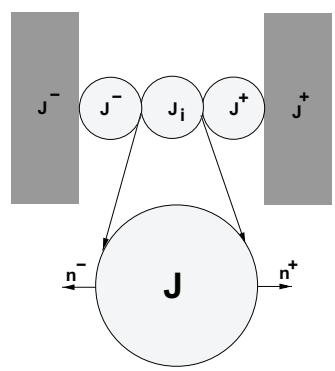

Figure 6. A one-dimensional example of current flow.

5.2. Iterative flux summation/solution process

The preceding relations lead to an implicit set of equations which are strongly coupled, as well as being coupled to the system dynamics. In order to deal with system, we employ a staggering scheme where, broadly speaking, the solution method sweeps through the system, *particle by particle*, updating the variables as it progresses. Specifically (where $K = 1, 2, \ldots$ is an iteration counter), the current is solved iteratively:

$$J_i^{K+1} = \frac{\sum_{j=1}^{N_{pc}} J_j^K A_{ij}^{cK}}{\sum_{j=1}^{N_{pc}} A_{ij}^{cK}}. \tag{43}$$

This process is repeated for all particles. The dynamical and thermo-mechanical equations are then re-solved for the motion and temperature of the particles *freezing the electrical current variables*, and the entire procedure (all previous steps) is repeated.

Remark 1: Once the current in each particle is solved for, one can compute the Joule-heating via $\mathcal{H}_i \approx a \frac{J_i^2}{\sigma_i} V_i$.

Remark 2: The particles in contact with the compacting walls/boundaries are assumed to become fully electrified and to attain the magnitude of current in the plate. From that particle, the current flows radially to other particles in contact at their respective contact points (Figure 5).

Remark 3: For an overview of the continuum modeling of current flow, Joule-heating, and so forth, see Zohdi [2, 3].

Remark 4: As an example, consider the one-dimensional array of particles shown in Figure 6. The two outer particles attain the values at the wall (due to the adopted approach for applying boundary conditions). According to the model, any current in a particle flows radially outward from the contact point into the neighboring particle.

Thus, for particle i we have two contact points

$$\begin{aligned}\sum_{j=1}^{2}(\boldsymbol{J}_i+\boldsymbol{J}_j)\cdot\boldsymbol{n}_{ij}A_{ij}^{c} &= (\boldsymbol{J}^{+}\cdot\boldsymbol{n}^{+}+\boldsymbol{J}_i\cdot\boldsymbol{n}^{+})A^{c,+}+(\boldsymbol{J}^{-}\cdot\boldsymbol{n}^{-}+\boldsymbol{J}_i\cdot\boldsymbol{n}^{-})A^{c,-}\\ &= (-J^{+}+J_i)A^{c,+}+(-J^{-}+J_i)A^{c,-}\\ &= 0.\end{aligned} \tag{44}$$

If the contact areas are the same, this collapses to the average, $J_i = \frac{1}{2}(J^{+}+J^{-})$.

6. Total system coupling: Multiphysical staggering scheme

We now extend the iterative solution process introduced earlier for the particle dynamics to a multifield setting by (at a given time increment): (a) solving each field equation individually, "freezing" the other (coupled) fields in the system, allowing only the primary field to be active, and (b) updating the primary field variable after the solution of each field equation. The next field equation is treated in a similar manner where, as the physics change, the field that is most sensitive (exhibits the largest amount of relative nondimensional change) dictates the time-step size. This is an implicit, staggered, adaptive time-stepping scheme.

Remark 1: Such approaches have a long history in the computational mechanics community. For example, Zienkiewicz [79], Zienkiewicz et al. [80], Lewis et al. [81], Lewis and Schrefler [82], Park and Felippa [83], Farhat et al. [84], Farhat and Lesoinne [85], Farhat et al. [86], Piperno [87], Piperno et al. [88], Piperno and Farhat [89], Michopoulos et al. [90], Lesoinne and Farhat [91] and Le Tallec and Muoro [92].

Remark 2: The particle currents are not explicitly used for the time adaptivity, since they are assumed to stabilize rapidly enough, relative to the dynamical and thermodynamical fields, that the steady-state equations can be used (see previous section and the Appendix).

6.1. A general iterative framework

We now further develop the staggering scheme introduced earlier by extending approaches found in Zohdi [77, 78] by considering an abstract setting, whereby one solves for the particle positions, assuming the thermal fields fixed,

$$\mathcal{A}_1(\underline{\boldsymbol{r}^{L+1,K}},\theta^{L+1,K-1}) = \mathcal{F}_1(\boldsymbol{r}^{L+1,K-1},\theta^{L+1,K-1}), \tag{45}$$

then one solves for the thermal fields, assuming the particle positions fixed,

$$\mathcal{A}_2(\boldsymbol{r}^{L+1,K},\underline{\theta^{L+1,K}}) = \mathcal{F}_2(\boldsymbol{r}^{L+1,K},\theta^{L+1,K-1}), \tag{46}$$

where only the underlined variable is "active," L indicates the time-step and K indicates the iteration counter. Within the staggering scheme, implicit time-stepping methods, with time-step size adaptivity, will be used throughout the upcoming analysis. We define the normalized errors within each time-step, for the two fields,

$$\varpi_{rK} \stackrel{\text{def}}{=} \frac{||\boldsymbol{r}^{L+1,K}-\boldsymbol{r}^{L+1,K-1}||}{||\boldsymbol{r}^{L+1,K}-\boldsymbol{r}^{L}||} \quad \text{and} \quad \varpi_{\theta K} \stackrel{\text{def}}{=} \frac{||\theta^{L+1,K}-\theta^{L+1,K-1}||}{||\theta^{L+1,K}-\theta^{L}||}. \tag{47}$$

We define maximum "violation ratio," i.e. as the larger of the ratios of each field variable's error to its corresponding tolerance, by $Z_K \stackrel{\text{def}}{=} max(z_{rK}, z_{\theta K})$, where

$$z_{rK} \stackrel{\text{def}}{=} \frac{\varpi_{rK}}{TOL_r} \quad \text{and} \quad z_{\theta K} \stackrel{\text{def}}{=} \frac{\varpi_{\theta K}}{TOL_\theta}, \tag{48}$$

with the minimum scaling factor defined as $\Lambda_K \stackrel{\text{def}}{=} min(\Lambda_{rK}, \Lambda_{\theta K})$, where

$$\Lambda_{rK} \stackrel{\text{def}}{=} \left(\frac{(\frac{TOL_r}{\varpi_{r0}})^{\frac{1}{pK_d}}}{(\frac{\varpi_{rK}}{\varpi_{r0}})^{\frac{1}{pK}}}\right), \qquad \Lambda_{\theta K} \stackrel{\text{def}}{=} \left(\frac{(\frac{TOL_\theta}{\varpi_{\theta 0}})^{\frac{1}{pK_d}}}{(\frac{\varpi_{\theta K}}{\varpi_{\theta 0}})^{\frac{1}{pK}}}\right). \tag{49}$$

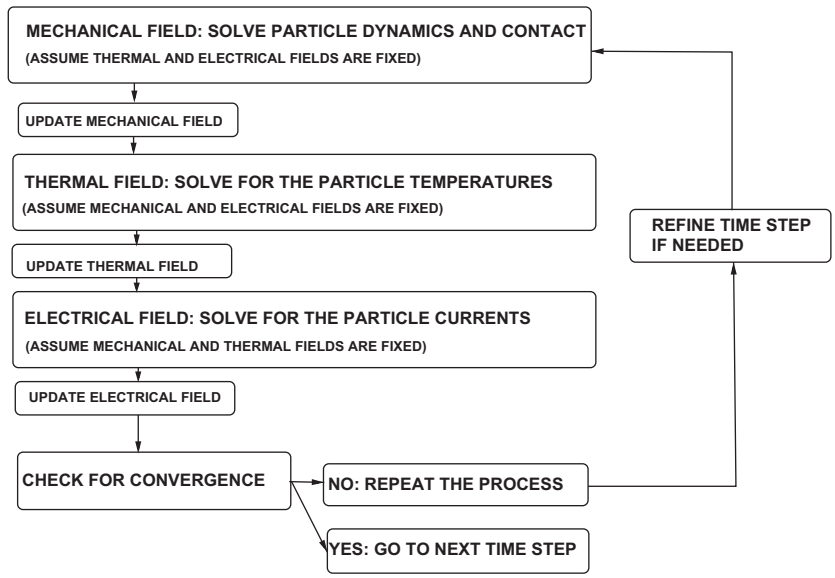

Figure 7. A flow chart for the modular, staggered, computation.

6.2. Overall solution algorithm

The algorithm is given in Algorithm 1 and the process visualized in Figure 7.

(1) GLOBAL FIXED − POINT ITERATION : (SET i = 1 AND K = 0) :
(2) IF i > N_p THEN GO TO (4)
(3) IF i ≤ N_p THEN : (FOR PARTICLE i)
  (a) COMPUTE POSITION :$\boldsymbol{r}_i^{L+1,K}$
  (b) COMPUTE TEMPERATURE :$\theta_i^{L+1,K}$
  (c) GO TO (2) AND NEXT PARTICLE (i = i + 1)
(4) ERROR MEASURES(normalized) :

$$(a)\varpi_{rK} \stackrel{\text{def}}{=} \frac{\sum_{i=1}^{Np} ||\boldsymbol{r}_i^{L+1,K} - \boldsymbol{r}_i^{L+1,K-1}||}{\sum_{i=1}^{Np} ||\boldsymbol{r}_i^{L+1,K} - \boldsymbol{r}_i^{L}||}$$

$$\varpi_{\theta K} \stackrel{\text{def}}{=} \frac{\sum_{i=1}^{Np} ||\theta_i^{L+1,K} - \theta_i^{L+1,K-1}||}{\sum_{i=1}^{Np} ||\theta_i^{L+1,K} - \theta_i^{L}||}$$

$$(b)Z_K \stackrel{\text{def}}{=} max(z_{rK}, z_{\theta K}) \quad where \quad z_{rK} \stackrel{\text{def}}{=} \frac{\varpi_{rK}}{TOL_r}, \qquad z_{\theta K} \stackrel{\text{def}}{=} \frac{\varpi_{\theta K}}{TOL_\theta}$$

$$(c)\Lambda_K \stackrel{\text{def}}{=} min(\Lambda_{rK}, \Lambda_{\theta K}) \quad where$$

$$\Lambda_{rK} \stackrel{\text{def}}{=} \left(\frac{(\frac{TOL_r}{\varpi_{r0}})^{\frac{1}{pK_d}}}{(\frac{\varpi_{rK}}{\varpi_{r0}})^{\frac{1}{pK}}} \right),$$

$$\Lambda_{\theta K} \stackrel{\text{def}}{=} \left(\frac{(\frac{TOL_\theta}{\varpi_{\theta 0}})^{\frac{1}{pK_d}}}{(\frac{\varpi_{\theta K}}{\varpi_{\theta 0}})^{\frac{1}{pK}}} \right)$$

(5) IF TOL. NOT MET ($Z_K > 1$) AND $K < K_d$ REPEAT ITERATION ($K = K + 1$)
(6) IF TOL. MET ($Z_K \leq 1$) AND $K < K_d$ THEN :
  (a) INCREMENT TIME : $t = t + \Delta t$
  (b) CONSTRUCT NEW TIME STEP : $\Delta t = \Lambda_K \Delta t$,
  (c) SELECT MINIMUM : $\Delta t = MIN(\Delta t^{lim}, \Delta t)$
  (d) UPDATE CURRENT FIELD $\boldsymbol{J}_i$(FOR ALL PARTICLES ITERATIVELY)
  (e) AND GO TO (1)
(7) IF TOL. NOT MET ($Z_K > 1$) AND $K = K_d$ THEN :
  (a) CONSTRUCT NEW TIME STEP :$\Delta t = \Lambda_K \Delta t$
  (b) UPDATE CURRENT FIELD $\boldsymbol{J}_i$(FOR ALL PARTICLES ITERATIVELY)
  (c) RESTART AT TIME = t AND GO TO (1)

Algorithm 1. Global fixed-point iteration.

The overall goal is to deliver solutions where staggering (incomplete coupling) error is controlled and the temporal discretization accuracy dictates the upper limits on the time-step size (Δt^{lim}).

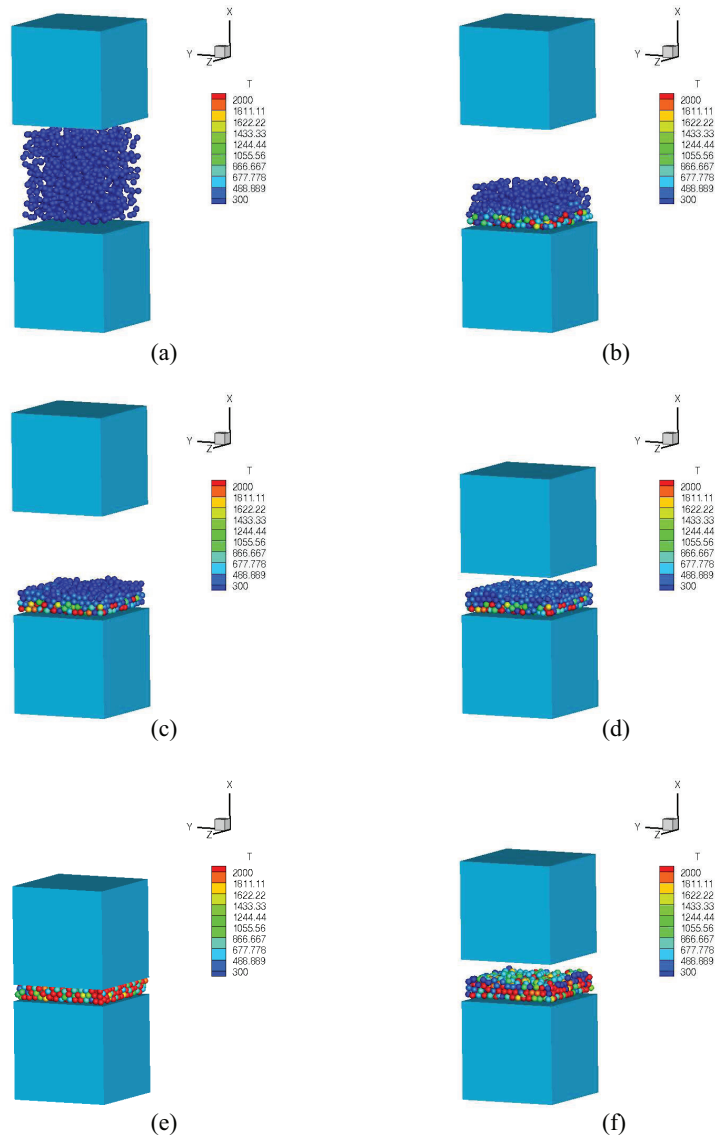

Figure 8. A series of frames for compaction using the model (side walls not shown). *Left* to *right* and *top* to *bottom*: (1) Pouring of the particles. (2) Contact with the lower electrified wall. (3) Contact with the upper and lower electrified wall. (4) Release of the upper electrified wall (loss of upper surface contact). The basic trends are: (a) the longer time the fully compressed state, the better the Joule-heating induced bonding and less springback; and (b) the higher the densification (higher volume-fraction) in the fully compressed state, the better the Joule-heating induced bonding and less springback. The volume fraction was calculated based on the volume contained within the lowest compression point in Figure 1.

7. Numerical examples

We consider a model problem of a group of equally sized particles placed between six walls (Figure 1) to illustrate how to assemble the system. The absolute dimensions are unimportant for the model problem, and have been normalized. Specifically, we considered a group of $N_p = 1000$ randomly positioned particles in initially cubical box domain with dimensions $(x = -1, x = 1) \times (y = -1, y = 1) \times (z = -1, z = 1)$ meters (the particles are then poured onto the lower wall. The particle radii were $R = 0.075$ m. In the x-direction (vertical), the top and bottom walls are electrified. The four other walls are neutral. The top is pushed downward at a constant rate (starting at $x = -1$), until it gets to $x = x^*$ at approximately 100% volume fraction, and then it is pulled away.[5] As an example, the relevant simulation parameters chosen were:

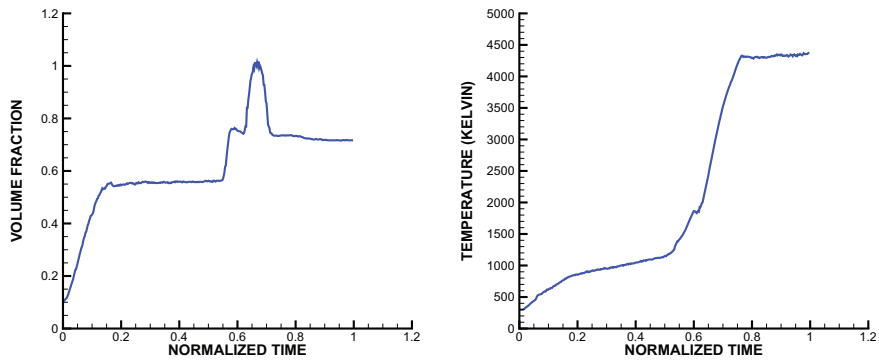

Figure 9. *The densification and temperature*: The process can be described as having three phases: phase (1): pouring to the roughly 50–60% volume fraction. The temperature rises due to contact with the lower electrified wall. phase (2): the compacting wall compresses the material to virtually 100% volume fraction. The temperature rises due to contact with the upper and lower electrified walls. phase (3): the compacting wall is released and the material springs back somewhat, resulting in a lower volume fraction than the fully compressed state, but higher than purely poured state. The temperature starts to drop due to conduction with the surrounding walls.

- the stiffness of the particles in the contact law were $K_{po} = 10^7$ N/m^2, with thermal softening $K_p = max(K_{po}\left(1 - \frac{\theta}{\theta^*}\right), K_p^{lim})$, where $\theta^* = 500°$K, $K_p^{lim} = 10^6$ N/m^2 and the exponent in the contact law was set to $p_p = 2$;
- the stiffness of the wall in contact law, $K_{wo} = 10^7$ N/m^2, with thermal softening $K_w = max(K_{wo}\left(1 - \frac{\theta}{\theta^*}\right), K_w^{lim})$, where $\theta^* = 500°$K, $K_p^{lim} = 10^6$ N/m^2 and the exponent in the contact law was set to $p_w = 2$;
- the bond stiffness, $K_b = 10^6$ N/m^2 and the exponent in the binding law was set to $p_b = 2$;
- the damping coefficient, $c^{env} = c_o^{env} 6\pi R$, $c_o^{env} = 0.1$ (assumed Stokesian-like);[6]
- the density of the particles, $\rho = 2000$ kg/m^3;
- the Joule-heating absorption coefficient, $a = 0.5$;
- the electrical conductivity, $\sigma = 0.1$;
- coefficient of dynamic friction, $\mu_d = 0.1$;
- conductivity (same for all particles in this example), $\mathbb{K} = 100$ W/m-K;
- initial material temperature, $\theta_i(t = 0) = 300°$K;
- wall temperatures, $\theta_w(t = 0) = 1000°$K;
- heat capacity, $C = 100$ J/kg-K;
- target number of fixed point iterations, $K_d = 10$;
- the trapezoidal time-stepping parameter, $\phi = 0.5$;
- on the bottom and top wall (in the x-direction), $J^{ext} = 10^5$ amps;
- simulation duration, 1 s;
- initial time-step size, 0.005 s;
- time-step upper bound, 0.005 s and
- tolerance for the fixed-point iteration, 5×10^{-4}.

7.1. Step 1: Pouring the particles

In order to generate an initial particle configuration, we dropped a sample of non-overlapping random particles onto the lower surface, and allowed it to spread under the force of gravity, where it was constrained by the lateral walls. The volume fraction of monodisperse random particles should be in range of 50-60% at this stage, and the simulation reflects that this is achieved before compaction, under the force of gravity (Figure 8).

Remark 1: The volume fraction was calculated based on the volume contained within the lowest compression point in Figure 1.

Remark 2: The configuration of the sample, before it was dropped, was generated using a classical Random Sequential Addition (RSA) algorithm [93], which places non-overlapping particles randomly into the domain

of interest. One could start with a denser starting configuration by the using equilibrium-driven Metropolis algorithm or alternative methods based on simultaneous particle flow and growth (see Kansaal et al. [21], Donev et al. [22–24] and Torquato [20]), although this was not necessary for this example.

7.2. Step 2: Compacting the particles

In Figure 8, the temperature values are depicted by the colors. Initially, the particles are not touching the electrified walls in the vertical (x-direction), nor the lateral, unelectrified walls. As the electrified wall moves in the (minus) x-direction, the particles come into contact, become electrified (experience a current) and move in the (minus) x-direction, as well as experience lateral movement (in the y–z) direction. The process can be described as having three phases:

- Phase 1: Pouring to the roughly 50–60% volume fraction. The temperature rises due to contact with the lower electrified wall.
- Phase 2: The compacting wall compresses the material to virtually 100% volume fraction. The temperature rises due to contact with the upper and lower electrified walls (Figure 9).
- Phase 3: The compacting wall is released and the material springs back somewhat, resulting in a lower volume fraction than the fully compressed state, but higher than purely poured state. For example, in the specific example chosen, the compaction process decreased the porosity by approximately 15% (Figure 9).

The basic trends are:

(a) the longer time the fully compressed state, the better the Joule-heating induced bonding and less springback; and
(b) the higher densification (higher volume-fraction) in the fully compressed state, the better the Joule-heating induced bonding and less springback.

8. Extensions and conclusions

This work developed a modular framework for the electrically enhanced sintering of powdered materials using a direct particle representation in conjunction with a staggering scheme to couple submodels of each type of physics together. The physics of this system are strongly coupled since the dynamics control which particles are in contact, which also dictates the electrical contacts, which in turn controls the Joule-heating and the induced thermal fields, which softens and binds the material. The strongly multiphysics-coupled sub-models were solved iteratively within each time-step using a staggering scheme which employs temporal adaptivity to control the error. The submodular approach allows for easy replacement of models, if so desired. Numerical examples were provided. There are a number of enhancements that can be made. For example, in general, the properties of most electrically active materials are quite sensitive to the temperature. For the conductivity, one can use the following decomposition, employing thermo-electric saturation conditions (using Sigmoid functions):

$$\sigma(\theta, \boldsymbol{E}) = \sigma(\theta_R, \boldsymbol{E}_R)\left(1 + \mathcal{K}_1(1 + e^{-\gamma_1(\theta-\theta_R)})^{-1} + \mathcal{K}_2(1 + e^{-\gamma_2||\boldsymbol{E}-\boldsymbol{E}_R||})^{-1}\right), \tag{50}$$

where the γ's and $\mathcal{K}$'s are material parameters, θ_R is a reference temperature, $\boldsymbol{E}$ is the electric field and $\boldsymbol{E}_R$ is the reference electrical state. Generally speaking, for many materials, until a saturation threshold is met, $\sigma(\theta)$ decreases with θ. See the treatise of Jackson [94] for reviews of the rich variety of possible dielectrical responses of materials, including atomistic-level discussions to motivate nonlinear dielectric behavior.

In closing, it is important to note that a significant acceleration in the computation can be achieved via sorting and binning methods, which proceed by partitioning the whole domain into bins (Figure 10). The particles are sorted by the bins in which they reside. The particle interaction proceeds, bin by bin, where the particles within a bin potentially only interact with particles in other nearest neighbor bins. Essentially, for a given particle in a bin, contact searches are conducted with particles in the neighboring bins only. The approach is relatively straightforward to implement and can speed up the computation dramatically (see Zohdi [78, 73]). There are a variety of related techniques to further accelerate computations. For example, one can assume that particles stay in the bins for a few time-steps, and that one does not need to re-sort immediately. One can construct so-called "interaction" or "Verlet" lists of neighboring particles which particles interact with, for a

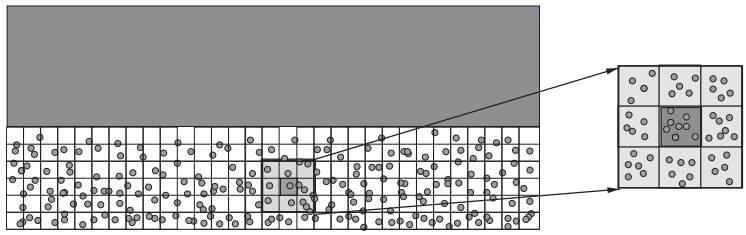

Figure 10. An example of binning of the particles in the sample domain.

few time-steps, and then update the interaction periodically (see Pöschel and Schwager [19]). One can also employ Domain Decomposition techniques whereby the domain is partitioned into subdomains, the particles within each subdomain are sent to a processor and stepped forward in time, but with the positions of the particles outside of the subdomain fixed (relative to the particles in that subdomain). This is done for all of the subdomains separately, then the position of all of the particles are updated and this information is shared between processors, with the process being repeated as needed. The use of these techniques is currently under investigation by the author.

Acknowledgments

The author expresses his gratitude to Mr Gary Merrill, Ms Cora Schillig and Dr Ramesh Subramanian of the Siemens corporation for support of this research.

Conflict of interest

None declared.

Funding

This research received partial funding from Siemens corporation.

Notes

1. The appendix gives a detailed analysis of Joule-heating phenomena.
2. Such forces can occur from viscous, surrounding, interstitial fluid.
3. The superscript L is a time interval counter.
4. $\mathbb{K}_{ij}$ can be approximated by an average interfacial value of the i–j pair, $\mathbb{K}_{ij} \approx \frac{\mathbb{K}_i + \mathbb{K}_j}{2}$. If the materials are the same, this collapses to simply $\mathbb{K}$. As for the mechanical contact, A^c_{ij} is the contact area associated with the particle pair (ij).
5. The transverse dimensions of the box were set to be approximately unity, initially. All system parameters can be scaled to describe any specific system of interest.
6. Prototypical values for c_o^{env} range from 0.1 to 10.

References

[1] Zohdi, TI. Estimation of electrical-heating load-shares for sintering of powder mixtures. *P Roy Soc A—Math Phy* 2012; 468: 2174–2190.
[2] Zohdi, TI. Simulation of coupled microscale multiphysical-fields in particulate-doped dielectrics with staggered adaptive FDTD. *Comput Method Appl M* 2010; 199: 79–101.
[3] Zohdi, TI. *Electromagnetic Properties of Multiphase Dielectrics. A Primer on Modeling, Theory and Computation*. Berlin, New York: Springer-Verlag, 2012.
[4] Demkowicz, L. *Computing with hp-Adaptive Finite Elements*. Vol. 1: *One and Two Dimensional Elliptic and Maxwell Problems*. Boca Raton, FL: Chapman & Hall/CRC, 2006.
[5] Demkowicz, L, Kurtz, J, Pardo, D, Paszynski, M, Rachowicz, W, and Zdunek, A. *Computing with hp-Adaptive Finite Elements*. Vol. 2: *Frontiers: Three Dimensional Elliptic and Maxwell Problems with Applications*. Boca Raton, FL: CRC Press, 2007.
[6] Akisanya AR, Cocks ACF and Fleck NA. The yield behavior of metal powders. *Int J Mech Sci* 1997; 39: 1315–1324.
[7] Anand, L, and Gu, C. Granular materials: Constitutive equations and shear localization. *J Mech Phys Solids* 2000; 48: 1701–1733.
[8] Brown, S, and Abou-Chedid, G. Yield behavior of metal powder assemblages. *J Mech Phys Solids* 1994; 42: 383–398.

[9] Domas F. Eigenschaftprofile und Anwendungsübersicht von EPE und EPP. Technical report of the BASF Company, 1997.
[10] Fleck, NA. On the cold compaction of powders. *J Mech Phys Solids* 1995; 43: 1409–1431.
[11] Gethin, DT, Lewis RW, and Ransing, RS. A discrete deformable element approach for the compaction of powder systems. *Model Simul Mater Sc* 2003; 11(1): 101–114.
[12] Gu, C, Kim, M, and Anand, L. Constitutive equations for metal powders: application to powder forming processes. *Int J Plasticity* 2001; 17: 147–209.
[13] Lewis, RW, Gethin, DT, Yang, XSS, and Rowe, RC. A combined finite-discrete element method for simulating pharmaceutical powder tableting. *Int J Numer Methods Eng* 2005; 62: 853–869.
[14] Ransing RS, Lewis RW and Gethin DT. Using a deformable discrete-element technique to model the compaction behaviour of mixed ductile and brittle particulate systems. *Philos T R Soc A* 2004; 362(1822): 1867–1884.
[15] Tatzel H. Grundlagen der Verarbeitungstechnik von EPP-Bewährte und neue Verfahren. Technical report of the BASF Company, 1996.
[16] Zohdi, TI. On the compaction of cohesive hyperelastic granules at finite strains. *P Roy Soc A—Math Phy* 2003; 454(2034): 1395–1401.
[17] Zohdi, TI. Genetic optimization of statistically uncertain microheterogeneous solids. *Philos T R Soc A* 2003; 361(1806): 1021–1043
[18] Duran, J. *Sands, Powders and Grains. An Introduction to the Physics of Granular Matter.* Springer-Verlag.
[19] Pöschel, T, and Schwager, T. *Computational Granular Dynamics*. New York: Springer-Verlag, 2004.
[20] Torquato, S. *Random Heterogeneous Materials: Microstructure and Macroscopic Properties*. New York: Springer-Verlag, 2002.
[21] Kansaal, A, Torquato, S, and Stillinger, F. Diversity of order and densities in jammed hard-particle packings. *Phys Rev E* 2002; 66(4/1): 041109.
[22] Donev A, Cisse I, Sachs, D, Variano, EA, Stillinger, F, Connelly, R, Torquato, S, and Chaikin, P. Improving the density of jammed disordered packings using ellipsoids. *Science* 2004; 13(303): 990–993.
[23] Donev, A, Stillinger, FH, Chaikin, PM, and Torquato, S. Unusually dense crystal ellipsoid packings. *Phys Rev Lett* 2004; 92: 255506.
[24] Donev, A, Torquato, S, and Stillinger, F. Neighbor list collision-driven molecular dynamics simulation for nonspherical hard particles. I. Algorithmic details. *J Comput Phys* 2005; 202: 737.
[25] Donev, A, Torquato, S, and Stillinger, F. Neighbor list collision-driven molecular dynamics simulation for nonspherical hard particles. II. Application to ellipses and ellipsoids. *J Comput Phys* 2005; 202: 765.
[26] Donev, A, Torquato, S and Stillinger, FH. Pair correlation function characteristics of nearly jammed disordered and ordered hard-sphere packings. *Phys Rev E* 2005; 71: 011105.
[27] Onate, E, Idelsohn, SR, Celigueta, MA, and Rossi, R. *Comput Method Appl M* 2008; 197(19–20): 1777–1800.
[28] Onate, E, Celigueta, MA, Idelsohn, SR, Salazar F and Suárez B. Possibilities of the particle finite element method for fluid-soil-structure interaction problems. *Comput Mech* 2011; 48: 307–318.
[29] Rojek, J, Labra, C, Su O and Onate, E. Comparative study of different discrete element models and evaluation of equivalent micromechanical parameters. *Int J Solids Struct* 2012; 49: 1497–1517. DOI: 10.1016/j.ijsolstr.2012.02.032.
[30] Carbonell, JM, Onate, E, and Suarez, B. Modeling of ground excavation with the particle finite element method. *J Eng Mech-ASCE* 2010; 136: 455–463.
[31] Labra C and Onate E. High-density sphere packing for discrete element method simulations. *Commun Numer Meth En* 2009; 25(7): 837–849.
[32] Jaeger, HM and Nagel, SR. La physique de l'etat granulaire. *Recherche* 1992; 249: 1380.
[33] Jaeger, HM and Nagel, SR. Physics of the granular state. *Science* 1992; 255: 1523.
[34] Nagel, SR. Instabilities in a sandpile. *Rev Mod Phys* 1992; 64: 321.
[35] Liu, CH, Jaeger, HM and Nagel, SR. Finite size effects in a sandpile. *Phys Rev A* 1991; 43: 7091.
[36] Liu CH and Nagel SR. Sound in a granular material: disorder and nonlinearity. *Phys Rev B* 1993; 48: 15646.
[37] Jaeger, HM, and Nagel, SR. La fisica del estado granular. *Mundo Cientifico* 1993; 132: 108.
[38] Jaeger, HM, Knight JB, Liu CH, and Nagel, SR. What is shaking in the sand box? *Mat Res Soc Bull* 1994; 19: 25.
[39] Jaeger, HM, Nagel SR, and Behringer, RP. The physics of granular materials. *Physics Today* 1996; 4: 32.
[40] Jaeger, HM, Nagel SR, and Behringer, RP. Granular solids, liquids and gases. *Rev Mod Phys* 1996; 68: 1259.
[41] Jaeger, HM, and Nagel, SR. Dynamics of granular material. *American Scientist* 1997; 85: 540.
[42] Tai, Y-C, Noelle S, Gray, JMNT, and Hutter K. Shock capturing and front tracking methods for granular avalanches. *J Comp Phys* 2002; 175: 269–301.
[43] Tai, Y-C, Gray, JMNT, Hutter, K , and Noelle, S. Flow of dense avalanches past obstructions. *Ann Glaciol* 2001; 32: 281–284.
[44] Tai Y-C, Noelle S, Gray JMNT and Hutter, K. An accurate shock-capturing finite-difference method to solve the Savage–Hutter equations in avalanche dynamics. *Ann Glaciol* 2001; 32: 263–267.
[45] Gray, JMNT, Wieland, M, and Hutter, K. Gravity-driven free surface flow of granular avalanches over complex basal topography. *P Roy Soc A—Math Phy* 1999; 455, 1841–1874.
[46] Wieland, M, Gray, JMNT, and Hutter, K. Channelized free-surface flow of cohesionless granular avalanches in a chute with shallow lateral curvature. *J Fluid Mech* 1999; 392: 73–100.

[47] Berezin, YA, Hutter, K, and Spodareva, LA. Stability properties of shallow granular flows. *Int J Nonlin Mech* 1998; 33(4): 647–658.
[48] Gray, JMNT, and Hutter, K. Pattern formation in granular avalanches. *Continuum Mech Therm* 1997; 9: 341–345.
[49] Gray, JMNT. Granular flow in partially filled slowly rotating drums. *J Fluid Mech* 2001; 441: 1–29.
[50] Hutter, K. Avalanche dynamics. In: Singh VP (ed) *Hydrology of Disasters*. Dordrecht, The Netherlands: Kluwer Academic Publishers, 1996, pp.317–394.
[51] Hutter, K, Koch, T, Plüss, C, and Savage, SB. The dynamics of avalanches of granular materials from initiation to runout. Part II: Experiments. *Acta Mech* 1995; 109: 127–165.
[52] Hutter, K, and Rajagopal, KR. On flows of granular materials. *Continuum Mech Therm* 1994; 6: 81–139.
[53] Koch, T, Greve, R, and Hutter, K. Unconfined flow of granular avalanches along a partly curved surface. II. Experiments and numerical computations. *P Roy Soc A—Math Phy* 1994; 445: 415–435.
[54] Greve, R, and Hutter, K. Motion of a granular avalanche in a convex and concave curved chute: Experiments and theoretical predictions. *Philos T R Soc A* 1993; 342: 573–600.
[55] Hutter, K, Siegel, M, Savage, SB, and Nohguchi, Y. Two-dimensional spreading of a granular avalanche down an inclined plane. Part I: Theory. *Acta Mech* 1993; 100: 37–68.
[56] Behringer, RP. The dynamics of flowing sand. *Nonlinear Sci Today* 1993; 3: 1.
[57] Behringer, RP, and Baxter, GW. Pattern formation, complexity and time-dependence in granular flows. In: Mehta A (ed.) *Granular Matter—An Interdisciplinary Approach*. New York: Springer-Verlag, 1993, pp.85–119.
[58] Behringer, RP, and Miller, BJ. 1997 Stress fluctuations for sheared 3D granular materials. In: Behringer R and Jenkins J (eds) *Proceedings of the third international conference on powders and grains*, Durham, NC, 18–23 May 1997, pp.333–336. Balkema.
[59] Behringer, RP, Howell, D, and Veje, C. Fluctuations in granular flows. *Chaos* 1999; 9: 559–572.
[60] Jenkins, JT, and Strack, ODL. Mean-field inelastic behavior of random arrays of identical spheres. *Mech Mater* 1993; 16: 25–33.
[61] Jenkins, JT, and La Ragione, L. Particle spin in anisotropic granular materials. *Int J Solids Struct* 1999; 38, 1063–1069.
[62] Jenkins, JT, and Koenders, MA. The incremental response of random aggregates of identical round particles. *Eur Phys J E* 2004; 13: 113–123.
[63] Jenkins JT and Johnson D, La Ragione, L, and Makse, H. Fluctuations and the effective moduli of an isotropic, random aggregate of identical, frictionless spheres. *J Mech Phys Solids* 2005; 53, 197–225.
[64] Maxwell, JC. On the dynamical theory of gases. *Philos Trans Soc London* 1867; 157: 49.
[65] Maxwell, JC. *A Treatise on Electricity and Magnetism*. 3rd edition. Oxford: Clarendon Press, 1873.
[66] Rayleigh, JW. On the influence of obstacles arranged in rectangular order upon properties of a medium. *Phil Mag* 1892; 32: 481–491.
[67] Jikov, VV, Kozlov, SM, and Olenik, OA. Homogenization of differential operators and integral functionals. Springer-Verlag, 1994.
[68] Hashin, Z, and Shtrikman, S. A variational approach to the theory of effective magnetic permeability of multiphase materials. *J App Phys* 1962; 33(10): 3125–3131.
[69] Nemat-Nasser S and Hori M. *Micromechanics: Overall Properties of Heterogeneous Solids*. 2nd edition. Amsterdam: Elsevier, 1999.
[70] Ghosh, S. 2011 *Micromechanical Analysis and Multi-Scale Modeling Using the Voronoi Cell Finite Element Method*. Boca Raton, FL: CRC Press/Taylor & Francis.
[71] Ghosh S and Dimiduk D. *Computational Methods for Microstructure-Property Relations*. New York: Springer-Verlag, 2011.
[72] Zohdi, TI, and Wriggers, P. *Introduction to Computational Micromechanics*. Berlin: Springer-Verlag, 2008.
[73] Zohdi, TI. Numerical simulation of charged particulate cluster-droplet impact on electrified surfaces. *J Comp Phys* 2013; 233: 509–526.
[74] Wriggers, P. *Nonlinear Finite Element Analysis*. Berlin: Springer-Verlag, 2008.
[75] Wriggers, P. *Computational Contact Mechanics*. Hoboken, NJ: John-Wiley, 2002.
[76] Zohdi, TI. Computation of strongly coupled multifield interaction in particle-fluid systems. *Comput Method Appl M* 2007; 196: 3927–3950.
[77] Zohdi, TI. An adaptive-recursive staggering strategy for simulating multifield coupled processes in microheterogeneous solids. *Int J Numer Method Eng* 2002; 53: 1511–1532.
[78] Zohdi, TI. On the dynamics of charged electromagnetic particulate jets. *Arch Comput Method E* 2010; 17(2): 109–135
[79] Zienkiewicz, OC. Coupled problems and their numerical solution. In: Lewis RW, Bettes P and Hinton E (eds) *Numerical Methods in Coupled Systems*. Chichester, UK: Wiley, 1984, pp.35–58.
[80] Zienkiewicz, OC, Paul, DK, and Chan, AHC. Unconditionally stable staggered solution procedure for soil-pore fluid interaction problems. *Int J Numer Method Eng* 1988; 26: 1039–1055.
[81] Lewis, RW, Schrefler, BA, and Simoni, L. Coupling versus uncoupling in soil consolidation. *Int J Num Anal Method Geomech* 1992; 15: 533–548.
[82] Lewis, RW, and Schrefler, BA. *The Finite Element Method in the Static and Dynamic Deformation and Consolidation of Porous Media*. 2nd edition. Chichester, UK, New York: Wiley Press, 1998.
[83] Park, KC, and Felippa, CA. Partitioned analysis of coupled systems. In: Belytschko T and Hughes TJR (eds) *Computational Methods for Transient Analysis*. New York: Elsevier, 1983, pp. 157–219.

[84] Farhat C, Lesoinne M and Maman N. Mixed explicit/implicit time integration of coupled aeroelastic problems: Three-field formulation, geometric conservation and distributed solution. *Int J Numer Meth Fl* 1995; 21: 807–835.
[85] Farhat, C, and Lesoinne, M. Two efficient staggered procedures for the serial and parallel solution of three-dimensional nonlinear transient aeroelastic problems. *Comput Method Appl M* 2000; 182: 499–516.
[86] Farhat, C, van der Zee, G, and Geuzaine, P. Provably second-order time-accurate loosely coupled solution algorithms for transient nonlinear computational aeroelasticity. *Comput Method Appl M* 2006; 195: 1973–2001.
[87] Piperno, S. Explicit/implicit fluid/structure staggered procedures with a structural predictor and fluid subcycling for 2D inviscid aeroelastic simulations. *Int J Numer Meth Fl* 1997; 25: 1207–1226.
[88] Piperno, S, Farhat, C, and Larrouturou, B. Partitioned procedures for the transient solution of coupled aeroelastic problems. Part I: Model problem, theory, and two-dimensional application. *Comput Method Appl M* 1995; 124(1–2): 79–112.
[89] Piperno S and Farhat C. Partitioned procedures for the transient solution of coupled aeroelastic problems. Part II: Energy transfer analysis and three-dimensional applications. *Comput Method Appl M* 2001; 190: 3147–3170.
[90] Michopoulos, G, Farhat, C, and Fish, J. Survey on modeling and simulation of multiphysics systems, *J Comput Inf Sci Eng* 2005; 5(3): 198–213.
[91] Lesoinne, M, and Farhat, C. Free staggered algorithm for nonlinear transient aeroelastic problems. *AIAA J* 1998; 36(9): 1754–1756.
[92] Le Tallec, P, and Mouro, J. Fluid structure interaction with large structural displacements. *Comput Method Appl M* 2001; 190(24–25): 3039–3067.
[93] Widom, B. Random sequential addition of hard spheres to a volume. *J Chem Phys* 1966; 44: 3888–3894.
[94] Jackson, JD. *Classical Electrodynamics*. Third edition. New York: Wiley, 1998

Appendix A:. Joule-heating

A1. Characterizing electrical losses

The flow of current through materials usually leads to the phenomena of Joule-heating. To understand the phenomena, we consider a general electromagnetic system characterized by Faraday's Law

$$\nabla \times \boldsymbol{E} = -\frac{\partial \boldsymbol{B}}{\partial t} \tag{51}$$

and Ampere's Law

$$\nabla \times \boldsymbol{H} = \frac{\partial \boldsymbol{D}}{\partial t} + \boldsymbol{J} \tag{52}$$

where we recall that $\boldsymbol{E}$ is the electric field, $\boldsymbol{D}$ is the electric field flux, $\boldsymbol{J}$ is the electric current, $\boldsymbol{H}$ is the magnetic field and $\boldsymbol{B}$ is the magnetic field flux. Joule-heating can be motivated by forming the inner product of the magnetic field with Faraday's law and the inner product of the electric field with Ampere's law and forming the difference to yield

$$\underbrace{\boldsymbol{E} \cdot (\nabla \times \boldsymbol{H}) - \boldsymbol{H} \cdot (\nabla \times \boldsymbol{E})}_{-\nabla \cdot (\boldsymbol{E} \times \boldsymbol{H}) = -\nabla \cdot \boldsymbol{S}} = \boldsymbol{E} \cdot \boldsymbol{J} + \underbrace{\boldsymbol{E} \cdot \frac{\partial \boldsymbol{D}}{\partial t} + \boldsymbol{H} \cdot \frac{\partial \boldsymbol{B}}{\partial t}}_{= \frac{\partial \mathcal{W}}{\partial t}}, \tag{53}$$

where $\mathcal{W} = \frac{1}{2}(\boldsymbol{E} \cdot \boldsymbol{D} + \boldsymbol{H} \cdot \boldsymbol{B}) = \frac{1}{2}(\boldsymbol{E} \cdot \boldsymbol{\epsilon} \cdot \boldsymbol{E} + \boldsymbol{H} \cdot \boldsymbol{\mu} \cdot \boldsymbol{H})$ is the electromagnetic energy and where $\boldsymbol{S} = \boldsymbol{E} \times \boldsymbol{H}$ is the Poynting vector. Thus

$$\frac{\partial \mathcal{W}}{\partial t} + \nabla \cdot \boldsymbol{S} = -\boldsymbol{J} \cdot \boldsymbol{E} \tag{54}$$

equation (54) is usually referred to as Poynting's theorem, and can be interpreted, *for simple material laws, where the previous representation for $\mathcal{W}$ holds*, as stating that the rate of change of electromagnetic energy within a volume, plus the energy flowing out through a boundary, is equal to the negative of the total work done by the fields on the sources and electrical conduction.

A2. Joule-heating

The interconversions of various forms of energy (electromagnetic, thermal, etc) in a system are governed by the first law of thermodynamics, for example case in the current configuration

$$\rho \dot{w} - \boldsymbol{T} : \nabla \dot{\boldsymbol{v}} + \nabla \cdot \boldsymbol{q} - Z = 0, \tag{55}$$

where ρ is the mass density in current configuration, w is the stored energy per unit mass, $\boldsymbol{T}$ is Cauchy stress, $\boldsymbol{v}$ is the material velocity and $\boldsymbol{q}$ is heat flux. We consider the absorbed energy that is available for heating to be proportional to the energy associated with electrical conduction, namely, from equation (54), $\boldsymbol{J} \cdot \boldsymbol{E}$, and account for it via $Z \stackrel{\text{def}}{=} \rho z = a\boldsymbol{J} \cdot \boldsymbol{E}$, where a is an absorption constant, $0 \leq a \leq 1$. *The systems considered in the body of the paper are special cases of this general continuum formulation, which was treated in Zohdi [2].*

Appendix B:. Time-scaling arguments for $\frac{\partial \mathcal{P}}{\partial t} \approx 0$

Consider the following

$$\int_{\partial\Omega} \boldsymbol{J} \cdot \boldsymbol{n}\, dA + \int_{\Omega} \frac{\partial \mathcal{P}}{\partial t}\, dV = 0 \Rightarrow \nabla \cdot \boldsymbol{J} = 0. \tag{56}$$

where $\frac{\partial \mathcal{P}}{\partial t} = 0$ is assumed the current propagates through the particles at a much faster time-scale than the deformation of the system. The velocity of the deformation of the system is far slower that the relative movement of charge (propagation of electricity) through the system (which is considered instantaneous). Changes in $\mathcal{P}$ are determined by the Gauss' law:

$$\int_{\partial\Omega} \boldsymbol{D} \cdot \boldsymbol{n}\, dA = \int_{\Omega} \mathcal{P}\, dV, \tag{57}$$

where $\boldsymbol{D}$ is the electric field flux. As an illustrative example, in order to appreciate the fast time scales that justify $\frac{\partial \mathcal{P}}{\partial t} \approx 0$, consider an arbitrary piece of continuum (undergoing no deformation) governed by

$$\nabla \cdot \boldsymbol{J} = \sigma \nabla \cdot \boldsymbol{E} = \frac{\sigma}{\epsilon} \nabla \cdot \boldsymbol{D} = \frac{\sigma}{\epsilon} \mathcal{P} = -\frac{\partial \mathcal{P}}{\partial t}, \tag{58}$$

where the following simple constitutive laws were used for illustration purposes: $\boldsymbol{J} = \sigma \boldsymbol{E}$, $\boldsymbol{D} = \epsilon \boldsymbol{E}$ and $\nabla \cdot \boldsymbol{D} = \mathcal{P}$. Solving for $\mathcal{P}$ yields

$$\mathcal{P}(\boldsymbol{x}, t) = \mathcal{P}(\boldsymbol{x}, t = 0) e^{-\frac{\sigma}{\epsilon} t}, \tag{59}$$

thus

$$\frac{\partial \mathcal{P}}{\partial t} = -\frac{\sigma}{\epsilon} e^{-\frac{\sigma}{\epsilon} t}. \tag{60}$$

The term $e^{-\frac{\sigma}{\epsilon} t}$ is extremely small since the ratio $\frac{\sigma}{\epsilon}$ is huge for the materials of interest and $-\frac{\sigma}{\epsilon} e^{-\frac{\sigma}{\epsilon} t} \approx 0$ for virtually any time-scales of interest, thus justifying $\int_{\partial\Omega} \boldsymbol{J} \cdot \boldsymbol{n}\, dA = 0$. In summary, any changes in $\mathcal{P}$ can be considered instantaneous, relative to mechanically induced deformations.